Precision Table-Top Portable Thermal Chamber with Double Thermoelectric Module

ANDERSON W. SPENGLER
UNICAMP
DEMIC
Av. Albert Einstein, 400
13083-852 Campinas, SP
BRAZIL
spengler@demic.fee.unicamp.br

ELNATAN C. FERREIRA
UNICAMP
DEMIC
Av. Albert Einstein, 400
13083-852 Campinas, SP
BRAZIL
elnatan@demic.fee.unicamp.br

JOSÉ A. SIQUEIRA DIAS
UNICAMP
DEMIC
Av. Albert Einstein, 400
13083-852 Campinas, SP
BRAZIL
siqueira@demic.fee.unicamp.br

Abstract: A portable thermal chamber with a volume of only 2.5 l capable of reaching temperatures over the $-5°$C to $70°$C range was designed and constructed. In order to make the thermal chamber lightweight and portable, two series connected thermoelectric modules were used as actuators since their size and performance characteristics allow the portability and precise temperature control. The PID control provided stability and errors better than normally found in expensive commercial thermal chambers, with maximum temperature error of $\pm 0.2°$C with respect to the setpoint and with a fluctuation of $\pm 0.1°$C.

Key–Words: Thermal chamber, Thermoelectric modules, Stacked Thermoelectric modules, Analogue PID, Temperature control, H-Bridge power driver.

1 Introduction

Commercial thermal chambers have a large volume, which makes them inappropriate for portable bench-top or field applications. The technology used in commercial thermal chambers employ compressors and radiators to cool down the chamber, requiring a lot of space and making them difficult to control with low steady-state temperature errors. To overcome these problems, this paper presents a technique where thermal electric modules (TEM) were used, making the equipment small and easier to control, resulting in a reduced size lightweight portable equipment that can be used in the field or in bench-top applications where precise temperature control are needed.

2 Design of the thermal chamber

The chamber size, insulation and materials are determinant in estimating the amount of power that will be required to cool or heat the chamber. The thermal chamber has the external dimensions of 300 mm x 240 mm x 120 mm and the internal space is 240 mm x 180 mm x 60 mm (approximately 2.6 l). The insulation is made of an elastomer foam with thermal conductivity of 0.037 W/(m.K) at $20°$C, and its thickness is only 30 mm.

To estimate the required power to cool the chamber, the AZTEC software [1] was used, and for the given dimensions and desired temperature, the program indicates that it is necessary 10.58 W, considering that an active internal load is dissipating 1W.

An interesting feature of this design is that two TEMs are used in a series configuration, in order to reduce the temperature difference between the ceramic plates and, therefore, allow for a higher heat transportation. The thermal chamber is built in two parts, which are united by a central element with two Teflon pieces in order to centralize the aluminum central parts. Fig. 1 shows the block diagram of the structure, the position of TEMs, sensors and copper blocks.

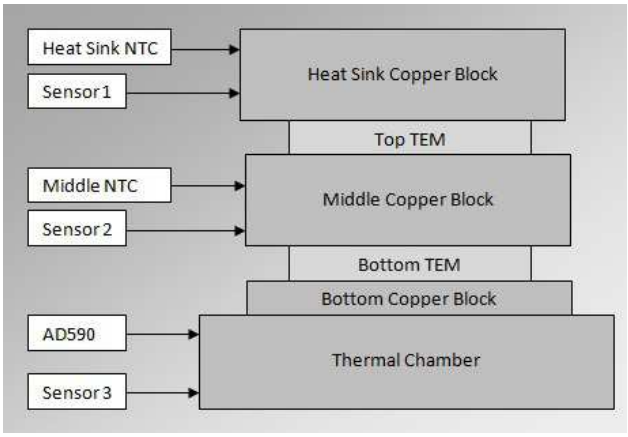

Figure 1: Actuators assembling diagram.

Since a critical part of TEM is dissipating the

ISBN: 978-1-61804-017-6

transported heat and the generated heat in this transportation, it was necessary to use a heat sink to remove the heat from the hot side of the top TEM. According to reference [2], the used heat sink will be 15º C above room temperature for a 125W load. The final assembling of the thermal chamber is done by fastening into the inner piece the module composed by the TEMs, copper blocks, heat sink, sensors and insulator. After this, the internal fan (required to make the spacial distribution of the heat more uniform and equalize the internal temperature) and the heat sink are also fixed in the inner piece. A photograph of the constructed thermal chamber with the temperature control board on its top is shown in Fig. 2.

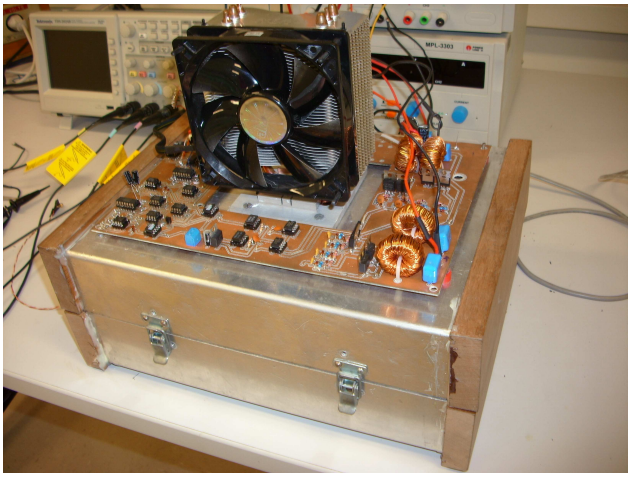

Figure 2: Thermal chamber constructed.

3 Eletronics Circuits

The block diagram of the thermal chamber circuits is presented in Fig. 5. The electronics circuits are used both to read the temperature (with digital integrated sensors) and to control the internal temperature by adequately driving the TEMs.

The microcontroller (PIC16F872A) [3] communicates with the interface module through a transceiver which has a galvanic insulation, the ADM2483 [4]. The digital temperature sensors employed were implemented with the LM95071 [5], which is a very fast and high resolution (12 bits) integrated temperature transducer. To measure the relative humidity inside de thermal chamber it was used a SHT15 [6]. Although it has the capability of measuring temperature, it was used only as a humidity sensor since is very slow and would jeopardize the performance of the temperature control. The setpoint voltage of the PID controller for the bottom TEM is determined by the user, and is internally generated with a 12 bits D/A converter with SPI communication

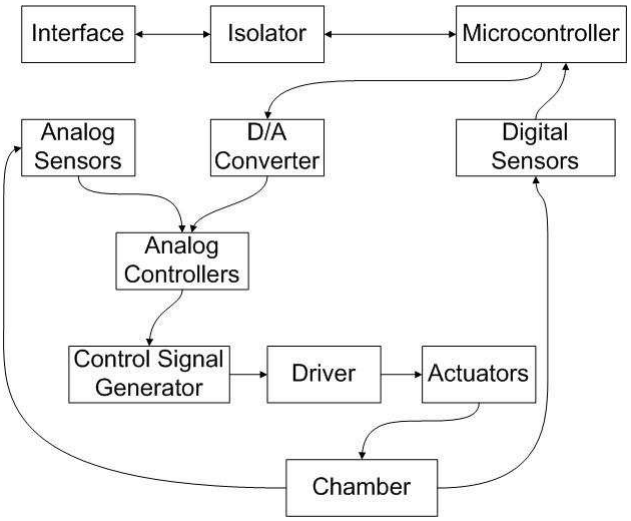

Figure 3: Block diagram of the thermal chamber circuits.

(TLV5616) [7].

The analogs sensors used are two 2.2 kΩ B57891M Series NTCs [8] and one AD590 [9]. The NTCs are fixed in the middle block and in the heat sink, since high precision is not required in these points. The AD590 is located inside the thermal chamber, where it is necessary a high accuracy in the temperature measurement. The three sensors signals are conditioned to present 32 mV/ºC, which is the same scale used in the D/A converter. In Fig. 4 the schematic diagram used in the signal conditioning of the NTCs is shown.

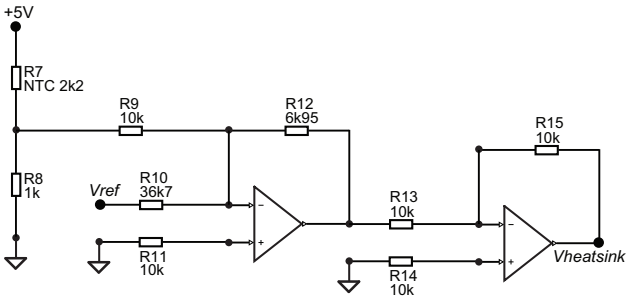

Figure 4: NTC signal conditioning circuit.

The AD590 signal conditioning circuit is presented in Fig. 5.

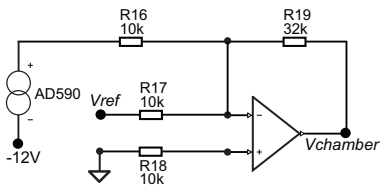

Figure 5: Conditioning circuit for the AD590.

The setpoint of the PID controller of the bottom

ISBN: 978-1-61804-017-6

TEM is determined by the user, and it is defined by a signal that comes from the D/A converter. To optimize the operation of the top TEM, its temperature setpoint is automatically chosen by the circuitry, and given by the following equation:

$$v_{setpoint} = 0.8v_{chamber} + 0.2v_{heatsink} \qquad (1)$$

where $v_{chamber}$ is the voltage related to chamber temperature and $v_{heatsink}$ is the voltage related to the heatsink temperature. This equation was obtained experimentally, measuring many TEM voltage configurations in order to obtain a higher cooling and heating efficiency.

The complete PID circuit of the bottom TEM is shown in Fig. 6. The choice of using an analog PID controller following the format proposed in [10] was due the low cost and good performance results which can be obtained with this circuit, so was unnecessary use a PID controller as describe in [11]. The PID parameters (proportional, integral and derivative gains) are adjusted individually and separately, offering more flexibility to the system. The summing amplifier can introduce signal attenuations of each signal coming from the PID main block.

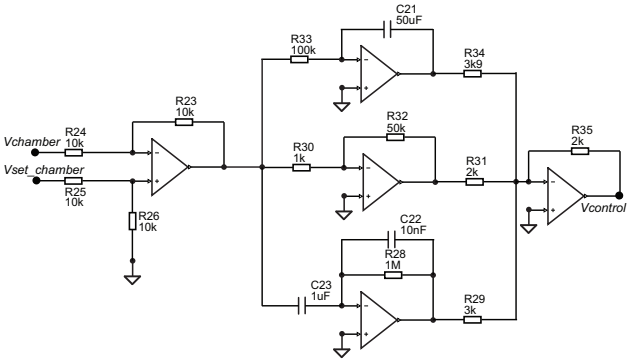

Figure 6: PID circuit used for the bottom TEM control.

Due to the high current required by the CP14-127-045 TEMs [12], an H bridge composed of MOSFET transistors driven by a PWM signal was used. To obtain the PWM signal, a conventional approach was adopted. A triangular wave with frequency $f_{\mathrm{PWM}} = 15$ kHz is generated and compared to the PID output signal. The output of the comparator is the required PWM signal.

The PWM signal is sent to the H bridge circuit through an optoisolator HCPL4503 [13], connected to two TC4428 [14] drivers, resulting in two complementary PWM signals outputs. To guarantee a continuous voltage level, LC filters are used in the output of the H bridge.

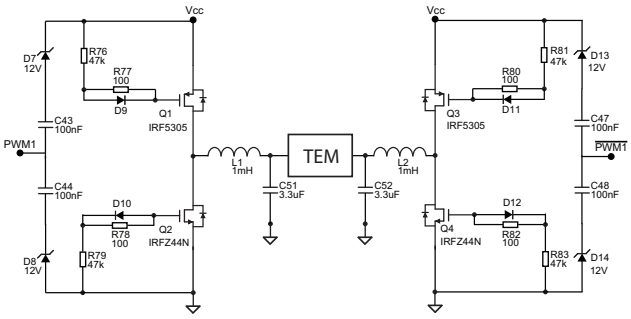

Figure 7: H bridge circuit.

4 Experimental results

The first test performed was to determine the minimum internal temperature that could be reached with the thermal chamber, driving the TEMs with a constant voltage source. The measured results are presented in Fig. 8. The test starts with a nitrogen flux inside the chamber, with 13 V and 6 A on the top and 5 V and 2.6 A on the bottom TEM. The relative humidity measured reaches -2%, but the sensor manufacturer [6] informs that negative values should be considered as zero. The nitrogen flow was turned off 150 minutes after the beginning of the test and an increase of the humidity is observed.

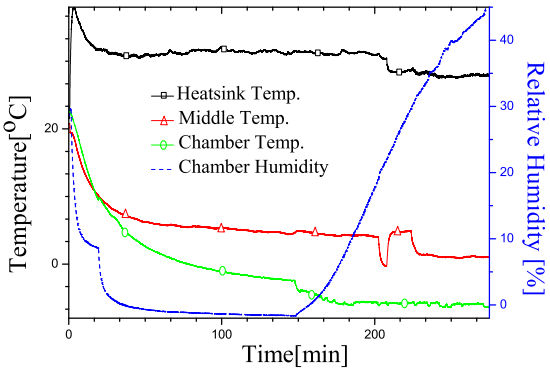

Figure 8: Measurement result to obtain the lowest temperature in the chamber.

At the end of the measurement cycle, the following temperatures were observed: $-6.4°$C inside the chamber, $1°$C in the intermediary block, and $27.8°$C at the heat sink. Using these values of measured temperatures and the graphs provided by [12], it was possible to estimate the transported power by each of the TEMs modules as about 20 watts for the top TEM (which is well above the 11 watts calculated by the manufacturer´s software) and around 30 watts for the bottom TEM, which is in agreement with the 28.8W predicted by the software.

The difference observed in the top TEM is justified by the unavoidable heat leakage from the cham-

ISBN: 978-1-61804-017-6

ber and also due to the insulation between the heat and cold sides of the TEM.

Due to the system nonlinearity in the heating and cooling process the PID tuning parameters were obtained experimentally. The optimal voltage for the bottom and top TEMs were also determined experimentally, after several experimental tests.

The traditional PID tuning method employed [15], is based in keeping only the proportional controlling part actuating, and then rising the proportional gain until the system starts to oscillate. The proportional gain is then set at 80% of this value. Secondly, using the found proportional gain, the integral and derivative gains are obtained in a similar way.

Table 1 - Gains obtained by the trial method.

Top TEM			
Gain	Kc	Ti	Tc
Value	20	17.625	2
Bottom TEM			
Gain	Kc	Ti	Tc
Value	49.9	9.8	0.664

A test with the chosen PID parameters with the set-point adjusted to $0°C$ is shown in Fig. 9, where the variation of the temperature as a function of the time is presented.

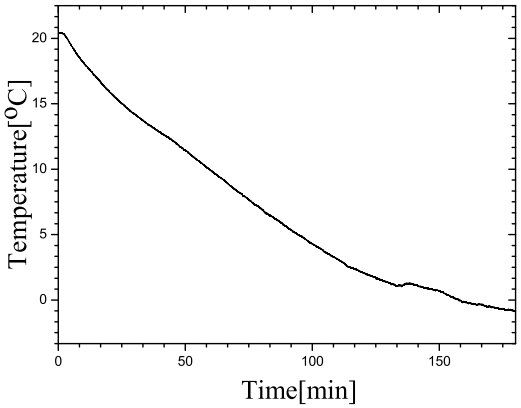

Figure 9: Variation of temperature with time when the thermal chamber is set to $0°C$.

The thermal chamber takes approximately 180 minutes to reach $-0.2°C$ and no overshoot is found. An excellent temperature stability is observed, as seen in Fig. 10. The gray lines are the temperature sensor measurements, which have a resolution of $0.03125°C$. It is important to notice that the maximum deviation is only around $0,16°C$. The black solid line shown is the result of the calculated average using the 10 previous and 10 subsequent points at each instant of time.

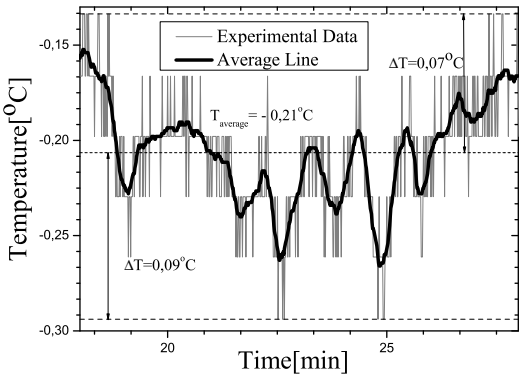

Figure 10: Temperature variation near $0°C$.

The upper proposed temperature limit for the thermal chamber is $70°C$. A test with the set-point set to this value is shown in Fig. 11. The response shows that a small overshoot ($2°C$) is verified, but the stability is soon reached. In the Fig. 11 is possible to see how the middle temperature follows the internal temperature as planned. Oscillations are also visible in the heatsink temperature, caused mainly by the room air conditioning action.

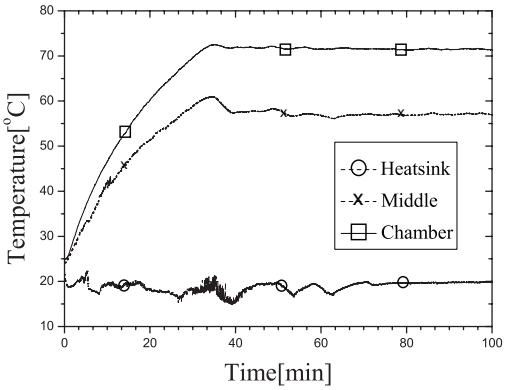

Figure 11: System temperature graph for $70°C$ set.

The temperature variation when the system is in steady state around $70°C$ is similar to that observed for $0°C$. This variation is approximately $0.16°C$, as shown in Fig. 12.

The Fig. 13 shows the transient response for various temperature set-points, showing that the system reaches its steady-state quickly when temperatures steps of $10°C$ are applied.

Although the option of using two TEMs in series has been made to allow the thermal chamber to reach lowest temperatures, it was observed that this configuration also improves the system´s response to external disturbances. This can be seen in Fig. 14, where

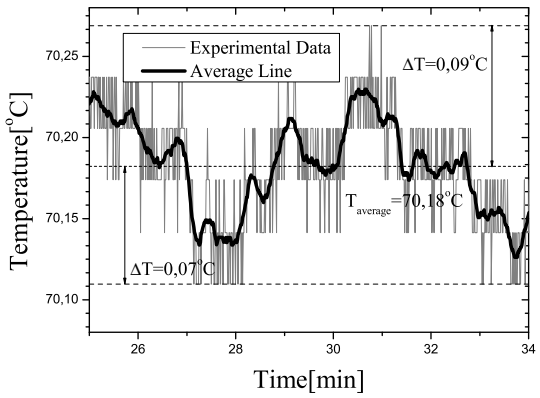

Figure 12: Internal temperature variation at 70°C.

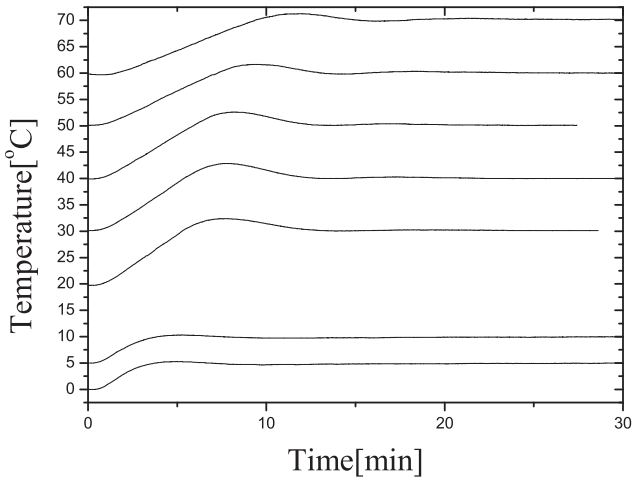

Figure 13: Temperature response for various set-points.

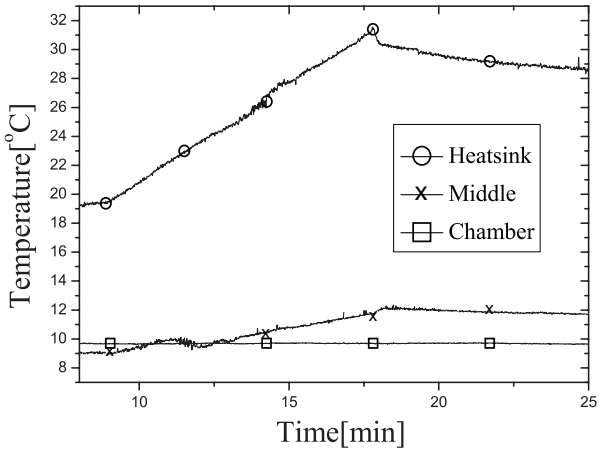

Figure 14: System reaction to an external disturbance.

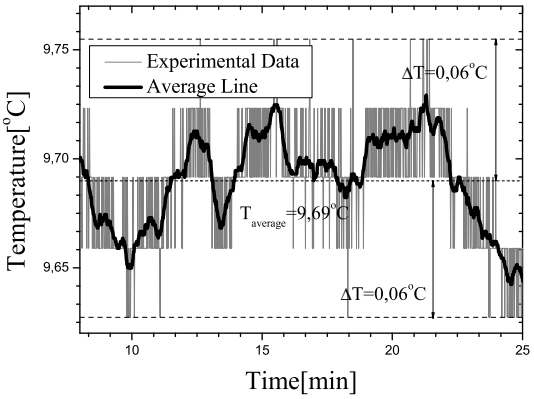

Figure 15: Internal temperature oscillation when an external disturbance is forced.

it is observed that an external disturbance in the heat sink temperature (provoked by turning off the external fan) affects only the intermediate temperature, and does not affect the internal temperature of the thermal chamber.

Fig. 15 shows the behavior of the internal temperature when an external disturbance is forced.

5 Conclusions

A low-cost and high performance table-top portable thermal chamber which covers the 0-70°C temperature range was designed and fabricated, using a double TEM technique. Due to its reduced volume and weight and the fact that it can be powered by two 12 V batteries, it can also be a valuable tool in field tests make possible field measurements.

The operation range of the thermal chamber is -5°C to 70°C, and an entrance for an inert gas like nitrogen allows the realization of tests below 0°C without condensation. The temperature fluctuation in steady state is only ± 0.1°C, and the relative temperature error to the set-point is ± 0.2°C, which outperforms most of the available commercial thermal chambers which are ten times more expensive.

References:

[1] Laird Technologies, *A-Z Thermoelectric Design*. Available: http://www.lairdtech.com/Products/AZTec-Software-Download/ [Accessed 20 November 2009]

[2] M. Page, *Akasa Nero AK-967 Heatsink Review*, 2009. Available: http//www.frosty-tech.com/articleview.cfm?articleID=2354 [Accessed 5 April 2010]

[3] Microchip Technology Inc., *PIC16F87XA Datasheet*. Available: http://ww1.microchip.com/downloads/en/DeviceDoc/39582b.pdf [Accessed 12 March 2009]

[4] Analog Devices Inc., *Half-Duplex, iCoupler, Isolated RS-485 Transceiver ADM2483 Datasheet*. Available: http://www.analog.com/static/imported-files/data_sheets/ADM2483.pdf [Accessed 12 March 2009]

[5] National Semiconductor Corp., *LM95071 Datasheet*. Available: http://www.national.com/pf/LM/LM95071.html [Accessed 15 March 2009]

[6] Sensirion AG, *Datasheet SHT1X*. Available: http://www.sensirion.com/en/pdf/product_information/Datasheet-humidity-sensor-SHT1x.pdf [Accessed 15 March 2009]

[7] Texas Instruments Inc., *TLV5616C, TLV5616I Datasheet*. Available: http://focus.ti.com/lit/ds/symlink/tlv5616.pdf [Accessed 12 March 2009]

[8] EPCOS, *NTC thermistors for temperature measurement Datasheet*. Available: http://www.epcos.com/inf/50/db/ntc_09/Leaded-Disks__B57891__M891.pdf [Accessed 15 March 2009]

[9] Analog Devices Inc., *2-Terminal IC Temperature Transducer AD590 Datasheet*. Available: http://www.analog.com/static/imported-files/data_sheets/AD590.pdf [Accessed 15 March 2009]

[10] C.C. Bradley, J. Chen and R.G. Huler, Instrumentation for the stable operation of laser diodes, *Rev. Sci. Instrum.* vol.61, n^{o}8, 1990, pp. 2097–2101.

[11] Shiuh-Jer Huang, Yi-Ho Lo, Metal Chamber Temperature control by Using Fuzzi PID Gain Auto-tuning strategy, *WSEAS Transactions on Systems and Control* vol.4, jan 2009, pp. 1-10.

[12] Laird Technologies, *Ceramic Plate Series CP14,127,045 Datasheet*. Available: http://www.lairdtech.com/WorkArea/linkit.aspx-?LinkIdentifier=id&ItemID=4291 [Accessed 13 March 2009]

[13] Avago Technologies, *HCPL-0452 0453 4502 4503 Datasheet*. Available: http://www.avagotech.com/docs/AV02-1392EN [Accessed 12 March 2009]

[14] Microchip Technology Inc., *TC4426 TC4427 TC4428 Datasheet*. Available: http://ww1.microchip.com/downloads/en/DeviceDoc/21422D.pdf [Accessed 22 March 2009]

[15] W.Y. Svrcek, D.P. Mahoney and B.R. Young, *A Real-Time Approach to Process Control*, Wiley, West Sussex, 2006.

[16] E. Flaxer, Implementnf of a precision fast thermoelectric cooler controller using a personal computer parallel port connection and ADN8830 controller, *Rev. Sci. Instrum.* vol.74, n^{o}8, 2003, pp. 3862–3873.

[17] A.W. Sloman, Comment on ”Implementing of a precision fast thermoelectric cooler using a personal computer parallel port connection and ADN8830 controller” [Rev. Sci. Instrum. 74, 3862 (2003)], *Rev. Sci. Instrum.* vol.75, n^{o}3, 2004, pp. 788–789.